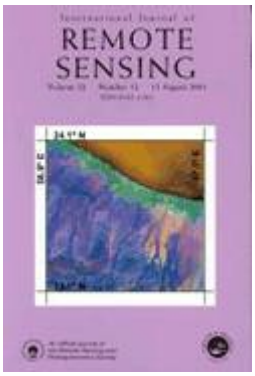

High resolution spatio-temporal water vapor mapping using GPS and MERIS observations

Journal:	*International Journal of Remote Sensing*
Manuscript ID:	TRES-SIP-2006-0011.R1
Manuscript Type:	Special Issue Paper
Date Submitted by the Author:	n/a
Complete List of Authors:	Lindenbergh, Roderik; Delft Institute of Earth Observation and Space Systems, Section Mathematical Geodesy and Positioning Keshin, Maxim; Delft Institute of Earth Observation and Space Systems, Section Mathematical Geodesy and Positioning van der Marel, Hans; Delft Institute of Earth Observation and Space Systems, Section Mathematical Geodesy and Positioning Hanssen, Ramon; Delft Institute of Earth Observation and Space Systems, Section Mathematical Geodesy and Positioning
Keywords:	DATA ANALYSIS, GEOSTATISTICS, MERIS, METEOROLOGY
Keywords (user defined):	MERIS GPS, water vapor, spatial-temporal combination
Note: The following files were submitted by the author for peer review, but cannot be converted to PDF. You must view these files (e.g. movies) online.	
revisionmerisremote.tex	

International Journal of Remote Sensing
Vol. 00, No. 00, DD Month 200x, 1–27

High resolution spatio-temporal water vapor mapping using GPS and MERIS observations.[c1]

RODERIK LINDENBERGH*, MAXIM KESHIN, HANS VAN DER MAREL AND RAMON HANSSEN

Delft Institute of Earth Observation and Space Systems, Delft University of Technology,

P.O. Box 5058, 2600 GB Delft, NL

(*Received 00 Month 200x; In final form 00 Month 200x*)

Improved knowledge of atmospheric water vapor and its temporal and spatial variability is of great scientific interest for climate research and weather prediction . Moreover, the availability of fine resolution water vapor maps is expected to reduce significant errors in applications using the Global Positioning System, GPS, or radar interferometry. Several methods exist to estimate water vapor using satellite systems. Combining radiances as measured in two spectral bands of the Medium Resolution Imaging Spectrometer (MERIS) results in an Integrated Water Vapor (IWV) product with high spatial resolution, up to 300 m, but a limited temporal resolution of about three days, in case of cloud free conditions. On the other hand, IWV estimates can be derived from the zenith total delays as observed by continuous GPS networks. The GPS IWV estimates have a higher temporal resolution of typically 1 hour, but, even in Western Europe, inter-station distances are at least tenths of kilometers. Here we describe how to obtain IWV products with high spatio-temporal resolution by combining GPS and MERIS IWV estimates. For this purpose an analysis is made of MERIS and GPS based IWV data, retrieved at the same day over Western Europe. A variance-covariance analysis is performed and is subsequently applied to produce time series of combined high-resolution water vapor maps using Kriging. The research presented here is a first step towards near real-time fine resolution water vapor products.[c2]

Keywords: GPS, MERIS, Kriging, water vapor, high spatial and temporal resolution[c3]

[c1] *changed from:* Comparing and Combining water vapor data from GPS and MERIS.

*Corresponding author. Email: r.c.lindenbergh@tudelft.nl

International Journal of Remote Sensing
ISSN 0143-1161 print/ ISSN 1366-5901 online ©2005 Taylor & Francis Ltd
http://www.tandf.co.uk/journals
DOI: 10.1080/01431160xxxxxxxxxxxxx

[c2] *changed from:* , but also geodetic positioning applications using GPS and radar interferometry will benefit. In this article both a comparison and a combination is made of MERIS and GPS based integrated water vapor data, retrieved at the same day over Western Europe. For both signals a variance-covariance analysis is made, that is applied in producing a time series of combined water vapor maps by means of the geostatistical Kriging approach

[c3] *changed from:* spatial-temporal

1 Introduction

Water vapor is the atmosphere's dominant greenhouse gas (Cess, 2005; Soden et al., 2005). Besides accounting for a large part of Earth's natural greenhouse effect, gaseous water also condenses to form clouds, which act as an isolation layer for earth's boundary layer. Knowledge on water vapor values is not only essential for environmental issues but also for satellite measurements from the Global Positioning System (GPS), (Bevis et al., 1992), or (Interferometric) Synthetic Aperture Radar, (In)SAR, (Hanssen, 2001). GPS and SAR signals are delayed by water vapor while traversing the atmosphere. Unlike most other atmospheric gases, the distribution of water vapor[a4] varies strongly in space and time. The change in IWV above a fixed point at the Earth's surface can to some extent be described by Taylors frozen flow assumption, (Taylor, 1938). This hypothesis states that a random field, in this case the water vapor distribution, is transported as a whole by the mean wind. As wind velocities and directions vary with altitude, Taylors assumption is only of limited use for direct assessment of Integrated Water Vapor values. (Elgered et al., 2005) show that IWV fields change often significantly within a one-hour period.[a5] This makes it necessary to monitor IWV both at high spatial and temporal resolution. Several metereological and space-geodetic systems exist that can observe IWV, but no single system meets this spatio-temporal resolution requirement, (Bevis et al., 1992; Hanssen et al., 1999; Seemann et al., 2003). However, this problem can be overcome by combining IWV observations from suitable complimentary systems.[c6]

In this paper we consider the fusion of IWV estimates as obtained from the MERIS and GPS satellite systems. At GPS ground stations, the vertically[c1] Integrated Water Vapor (IWV) can be derived from the total tropospheric[a2] delay that the GPS signals undergo while traveling from the GPS satellites to the ground receivers. This derivation results in relatively accurate IWV estimates with a high temporal (e.g. 1 hour) but a low spatial resolution (tens to hundreds kilometers). The Medium Resolution Imaging Spectrometer (MERIS) is a push-broom imaging spectrometer with a maximum spatial resolution of 300 m.

[a4] *new text added*
[a5] *new text added*
[c6] *changed from:* Mapping the spatial distribution of water vapor in the atmosphere is difficult due to the limited spatial and temporal resolution of contemporary meteorological instrumentation. It is however also possible to retrieve water vapor estimations from different satellite systems, (Hanssen et al., 1999; Seemann et al., 2003).
[c1] *changed from:* zenith
[a2] *new text added*

It measures the solar radiation reflected by the Earth in 15 spectral bands, programmable in width and position, in the visible and near infra-red frequency domain. Although the main mission of MERIS is in oceanography, by observing sea-color, it also observes, amongst others, the water vapor column over land, water or above clouds. Observations are limited to the sun-side of the orbit.[a3] [r4] MERIS can observe dynamic structures on scales much smaller than possible before. Its temporal resolution however is restricted to 3 days. MERIS also retrieves cloud type and cloud top height.[a5]

Here we analyze MERIS and GPS IWV data over North-West Europe on an arbitrary single day, August 9, 2003. The GPS IWV observations consist of time series of data from 26 ground stations at a temporal resolution of less than an hour. The MERIS data from the same day, acquired shortly after 10 UTC, has a spatial resolution of 1.2 km. The correlation between the two data sources around the acquisition time of the MERIS image is determined by comparing a selected number of MERIS pixels to the GPS IWV estimates. An experimental variance-covariance analysis is performed for both data sets. In the MERIS case this analysis is spatial, in the GPS case it is both spatial and temporal. The two data sets are combined to produce time series of hourly water vapor maps incorporating their spatio-temporal covariances, (Goovaerts, 1997; Gneiting et al., 2007). Except for the water vapor maps itself, this procedure results in error maps, displaying the errors as propagated from the individual error components. These results express the expected gain from combining GPS and MERIS water vapor data, provided that there is a reasonably dense network of GPS ground stations, as can be found over e.g. Europe and North-America.[a1]

In Section 2 a short description of the algorithms used for estimating the IWV contents within the GPS and MERIS systems is given. In Section 3 it is explained how to obtain the spatial and temporal correlation between the different IWV observations and how to combine the observations for a prediction at a certain time and location. In Section 4 GPS and MERIS observations from August 9, 2003 are compared and combined. The paper finishes with discussion of the results and an outlook on further research in

[a3] *new text added*
[r4] *removed:* The MERIS instrument on the Envisat satellite estimates integrated water vapor by observing the backscatter of solar radiation in the near infrared over land, sea and above clouds. With a maximum spatial resolution of 300 m,
[a5] *new text added*
[a1] *new text added*

Section 5.

2 GPS and MERIS IWV data

r1

2.2 *GPS IWV*

In GPS data processing, measurements from all satellite signal paths are mapped onto the vertical direction by means of a pre-defined mapping function. In this way the effect of GPS path delay in the troposphere can be estimated.[c2] This effect is called the zenith tropospheric delay, denoted as D_T. Only the total effect can be directly estimated from GPS measurements in this way, although this is composed of two components. The zenith hydrostatic delay, D_H, is due to the neutral gases in the troposphere and the non-dipole part of water vapor, while the second component, the zenith wet delay, D_W, appears due to the dipole moment of water vapor.[c3] That is,

$$D_T = D_H + D_W. \quad (1)$$

[r1] *removed:*

2.1 *Integrated Water Vapor*

Water vapor is the gas phase of water. Gaseous water represents a small but environmentally significant constituent of the atmosphere. Most of it is contained in the boundary layer, the lowest 2 km of the troposphere. In this article we will consider columnar water vapor values. Such values are expressed in kg/m^2, that is as the mass of the water vapor contents in a column of atmosphere above a horizontal square patch of 1m × 1m on the Earth's surface.

The change in IWV above a fixed point of the Earth's surface can to some extend be described by Taylors frozen flow assumption, (Taylor, 1938). This hypothesis states that a random field, in our case the water vapor distribution, as a whole is transported by the mean wind. As wind velocities and directions vary with their height above the Earth's surface, Taylors assumption is of only limited use for direct assessment of Integrated Water Vapor Values. It is reported, (Elgered et al., 2005), that IWV fields often significantly change while traveling one hour upwind.

Knowledge on water vapor values is not only essential for environmental issues but also for satellite measurements from GPS and (In)SAR: the GPS or SAR signal is delayed by atmospheric water vapor.

[c2] *changed from:* delay above a GPS station can be estimated.

[c3] *changed from:* reflects the impact of dry air on the propagation of the GPS signal and depends on the surface pressure. The second, wet, component appears due to the presence of water vapor in the lower parts of the atmosphere.

Note that the tropospheric parameters in Eq. (1) have units of distance, i.e. meters. The zenith hydrostatic delay can be estimated using

$$D_H = 10^{-6} \cdot \frac{k_1 \cdot R_d \cdot P}{g_m} = \frac{0.0022767 \cdot P}{1 - 0.00266 \cos 2\varphi - 2.8 \cdot 10^{-7} H}, \quad (2)$$

where φ is the ellipsoidal latitude of the GPS station in rad, k_1 an empirical constant [77.604 $\pm$ 0.014 K mbar^{-1}, (Thayer, 1974)], R_d the gas constant of dry air [461.51 J kg^{-1} K^{-1}] and g_m the mean gravity in m s^{-2}. H indicates the orthometric station height in meters and P the surface air pressure in mbar. The zenith wet delay is then obtained from Eq. (1) and mapped into integrated water vapor, denoted I and expressed in kg m^{-2}, by means of the following expression:

$$Z_W = Q \cdot I, \quad (3)$$

where Q, a dimensionless quantity, is a function of the mean temperature of water vapor, (Klein Baltink et al., 2002).[c0]

GPS IWV processing. Zenith tropospheric delay is estimated along with many other parameters, such as station coordinates, etc., by GPS software suites like the Bernese GPS software, (Rothacher et al., 1996) and GIPSY-OASIS II, (Webb and Zumberge, 1993). This process can be performed both in near real-time and in post-processing mode with time resolutions down to 5–6 min. As every tropospheric estimate typically uses a batch of GPS measurements, the GPS IWV estimates represent in fact a time-averaged amount of water vapor above the receiver location.[a1] Numerous validation experiments show that an accuracy of 1-2 kg/m^2 IWV is achievable for both post-processed and near real-time GPS IWV estimates,

[c0] *changed from:* ZHD can be computed directly as follows

$$\mathrm{ZHD} = \frac{0.0022767 \cdot P}{1 - 0.00266 \cos 2\varphi - 2.8 \cdot 10^{-7} H}, \quad (4)$$

where φ is the ellipsoidal latitude of the GPS station, H the orthometric station height and P the surface pressure. ZWD is then obtained from Equation 1. Zenith wet delay can then be mapped into integrated precipitable water vapor (IWV) by means of the following expression:

$$\mathrm{IWV} = \Pi \cdot \mathrm{ZWD}, \quad (5)$$

where Π is about 0.15 and depends on the mean temperature of the atmosphere, (Klein Baltink et al., 2002).

[a1] *new text added*

see e.g. (Jarlemark et al., 2002; Klein Baltink et al., 2002; Elgered et al., 2005). The possibility to use data from GPS networks for operational meteorology has been demonstrated in the framework of the COST-716 project (Elgered et al., 2005), which took place in 2001-2004. In 2003, the period under consideration in this paper, ten European Analysis Centers were participating in that project, which involved processing a network of more than 350 stations covering the whole of Europe.

GPS area of influence. The IWV at a given GPS station at a given time is determined from a number of different signal paths, one for every visible GPS satellite, forming a hypothetical cone, see Figure 1. That is, the GPS IWV estimate represents the average of the cross section of the cone with the effective tropospheric boundary layer height. For the comparison to the MERIS observations, all MERIS pixels within this area of influence (AOI) are averaged. As the configuration of GPS satellites is continuously changing it is at first approach only possible to use an approximate AOI. In this paper we start from a rather simple circular AOI model, which is evidently imperfect. The reasons are twofold. First, GPS IWV estimates represent averaged rather than instantaneous amounts of water vapor. As a consequence, the circular AOI is distorted, e.g. elongated, because of wind-induced water vapor advection.[a1] Second, the AOI is affected by the gap in GPS satellite coverage towards the North of GPS ground stations on the Northern hemisphere and towards the South on the Southern hemisphere. Note that the area with no GPS satellite visibility in the sky is larger at higher latitudes. Instead of using a fully geometric approach depending on elevation cutoff and signal path geometries, we obtain an optimal radius R_{GPS} as follows. First an upper bound $R_U = 10/\arctan 10 \approx$ 58[c2] km for the radius is determined by combining the elevation cutoff angle of 10 degrees with an approximate height of the troposphere, were most water vapor is concentrated, of 10 km. As a measure of agreement between the two types of observations of the IWV, Pearson's correlation coefficient is used. We determine the correlation coefficient between the GPS IWV estimates and the MERIS IWV pixels within a distance R from the GPS stations varying between 0 and the upper bound $R_U = 58$ km in steps of 250 m.[c3] The value of R that gives the highest correlation is

[a1] *new text added*
[c2] *changed from:* 15
[c3] *changed from:* Let R vary between 0 and the upper bound R_U of 58[c4] km and determine in steps of 250 m the correlation coefficient between the GPS IWV estimates and the MERIS IWV pixels within distance R of the GPS stations.

chosen as the AOI radius R_{GPS}.

2.3 *MERIS IWV*

[r1]

Here, a short sketch of the MERIS IWV retrieval algorithm is given. More details, together with accuracies, can be found elsewhere, i.e. in (Bennartz and Fischer, 2001; Fischer and Bennartz, 1997).[a2] Integrated Water Vapor values are obtained by a differential absorption method from the radiances L_{14} and L_{15} measured in channels 14 and 15, resp. These channels are centered around 885 and 900 nm, with a half width value of ± 10 nm. The ESA algorithm to derive the IWV estimates, W, is based on the logarithmic relation

$$W = k_0 + k_1 \log \frac{L_{15}}{L_{14}} + k_2 \log^2 \frac{L_{15}}{L_{14}}, \tag{6}$$

between the columnar water vapor and the ratio of the spectral radiances from bands 15 and 14. The k_0, k_1 and k_2 are regression constants.

The values of the regression constants depend on the viewing geometry. Moreover, there are also differences in methodology for IWV estimates above land and water. The absorption of water is higher, therefore the aerosol scattering gains influence and is taken into account over water by including the values for the 'aerosol' channels 9, 12, and 13 in the determination of the regression constants. The theoretical accuracy of the estimated water vapor column is 1.7 kg/m^2 over land and 2.6 kg/m^2 over water at full resolution. The IWV accuracy at the reduced resolution of 1.2 km is specified to be at most 20 % of the IWV estimation[c3].

[r1] *removed:* Since its launch on board the Envisat satellite in March 2002, the Medium Resolution Imaging Spectrometer MERIS gives insight into the properties and dynamics of the Earth system with unprecedented accuracy and resolution. MERIS is a push-broom imaging spectrometer with a maximal spatial resolution of 300m. It measures the solar radiation reflected by the Earth in 15 spectral bands, programmable in width and position, in the visible and near infra-red. The main mission of MERIS is oceanography, observing sea-color. The secondary mission of MERIS is to observe, amongst others, the water vapor column over land, water or above clouds. Observations are limited to the day-side. Global coverage is obtained after 3 days. MERIS also retrieves cloud type and top height.

[a2] *new text added*

[c3] *changed from:* The specified accuracy for the IWV contents at the reduced resolution of 1.2 km is specified as smaller than 20%.

3 Integrating GPS and MERIS data.

3.1 *Spatial and temporal continuity.*

As follows from a frozen turbulence hypothesis, (Taylor, 1938), local fluctuations of water vapor in the troposphere are transported over a location with a constant wind speed, therefore water vapor measurements obtained at nearby locations and time moments are correlated.[a0] Correlation in time or in space between observations can be detected and modeled by a variogram or covariance analysis, (Goovaerts, 1997). This model is used to determine the (V)ariance-(C)ovariance matrices of the observations. Using the VC matrices, a Best Linear Unbiased Prediction can be obtained for the IWV content at a given time and location. The underlying assumption used in this framework is that the IWV can be considered as a random function $Z(x,t)$[a1], that is, every observation is one single outcome of a complete distribution of possible observations at location x and at time t. [r2] Given a set of observations, a discrete experimental covariance function is determined by computing experimental covariances between any two observations and by binning the outcomes in distance intervals. The distance intervals should be chosen such that a sufficient number of experimental covariance samples can be found in every bin. By fitting the bin-wise averages of the samples into a positive definite model, a continuous covariance function is obtained that is used to fill the VC-matrix for a prediction at arbitrary location or moment.[c3] The obtained spatial, $c_s(x)$, and temporal, $c_t(t)$ covariance functions are combined into a spatio-temporal covariance function $c(x,t)$. The underlying spatio-temporal random function is said to be *separable*, (Gneiting et al., 2007), if $c(x,t)$ can be written as

$$c(x,t) \;=\; c_s(x)\cdot c_t(t) \;=\; \frac{c(x,0)\cdot c(0,t)}{c(0,0)} \tag{8}$$

[a0] *new text added*

[a1] *new text added*

[r2] *removed:* Stationarity of a random function means that the expectation of the function value is independent of location or time. The theoretical covariance function of a stationary random function $Z(x)$ is an expectation, E, and is defined as

$$\mathrm{cov(s)} = \mathrm{E((Z(x)\text{-}m)(Z(x+s)\text{ - }m))}, \tag{7}$$

where $m = E(Z(x))$ denotes the mean of $Z(x)$ and s a temporal or spatial distance.

[c3] *changed from:* Given a set of observations, a discrete experimental covariance function can be determined by computing experimental covariances between any two observations and by grouping the outcomes according to some distance interval. By fitting the experimental values into a positive definite model, a continuous covariance function is obtained that is used to fill the VC-matrix for a prediction at an arbitrary location or moment.

Note that a separable covariance function is also *symmetric*, that is $c(x,t) = c(-x,-t)$, for any spatial difference x and any time difference t.[a4] Physically, an asymmetric spatio-temporal covariance function can be chosen to implement transport effects due to prevailing wind directions, that is, by incorporating Taylors frozen flow assumption.[a5] Here we adapt the separable case to be used as a starting point, as this is conceptually the easiest. Moreover, thorough comparisons show only a weak dependence of the quality of interpolation results on the type of the spatio-temporal covariance function in case of similar meteo data, (Gneiting et al., 2007).[a6]

Ordinary Kriging clustering and screening properties. Incorporating the variance-covariance structure of the observations into the interpolation method has two effects that do not occur in case of e.g. inverse distance interpolation, (Wackernagel, 2003; Chilès and Delfiner, 1999). *De-clustering* refers to the partition of weights over correlated observations. The *screening* effect occurs when one observation is behind another observation with respect to the prediction location; the observation behind contains limited new information, and will therefore obtain a low weight compared to the preferred observation in front.[c1] It is even possible that the observation behind receives a negative weight. The stress on the weights can be relieved by increasing the so-called *nugget value* or white noise. This value encodes the short time variability or the size of the measurements errors. The clustering and screening effect will have significant influence on the result, especially for the GPS IWV observations which are spatially sparse and not regularly spaced.

[a4] *new text added*
[a5] *new text added*
[a6] *new text added*
[c1] *changed from:* Incorporating the variance-covariance structure of the observations into the interpolation method has some important consequences, (Wackernagel, 2003; Chilès and Delfiner, 1999). Two interpolation effects occur that do not occur in case of e.g. inverse distance interpolation. The first effect is known as *clustering*. According to the spatial (or temporal) continuity assumption, close by observations will be highly correlated. This implies that the additional weight obtained by an extra observation in the direct neighborhood of an existing observation will be limited, as according to the high correlation, there is limited new information in the extra observation. This effect is called clustering because weights can be at first instance being thought of as being divided between the different clusters of observations rather than between individual observations.
The second effect is known as *screening* and can be thought of as happening within one cluster. If one observation is behind another observation with respect to the prediction location, the observation behind contains limited new information. Therefore it will obtain a low weight compared to the observation in front, that is preferred because it is closer to the prediction location.

3.2 *Spatio-temporal interpolation.*

The MERIS IWV observations have a high spatial resolution, but only one epoch of observations is available. On the other hand, the GPS IWV observations are spatially sparse but are available at regular time intervals. Therefore it is straightforward to estimate an IWV value $\hat{I}(t_G,(x,y))$ at time t_G and location $p_0=(x,y)$ as a linear combination

$$\hat{I}(t_G,p_0) = (w_1\cdot I_{G,1}(p_1,t_G)+\cdots+w_n\cdot I_{G,n}(p_n,t_G)) \quad + \quad v\cdot I_M(p_0,t_M) \tag{9}$$

of GPS IWV observations $I_{G,1}(p_1,t_G)$, ..., $I_{G,n}(p_n,t_G)$ made at n different locations at time t_G, and one MERIS IWV observation $I_M(p_0,t_M)$ at location p_0, obtained at time t_M. The weights $w_1,\ldots,w_n$ for the n GPS IWV observations and v for the one MERIS IWV observation are obtained by solving the following ordinary Kriging system.

$$\begin{pmatrix} c(0,0)+N & c(x_{12},0) & \ldots & c(x_{1n},0) & c(x_{10},t) & 1 \\ c(x_{12},0) & c(0,0)+N & \ldots & c(x_{2n},0) & c(x_{20},t) & 1 \\ \vdots & \vdots & \ddots & \vdots & \vdots & \vdots \\ c(x_{1n},0) & c(x_{2n},0) & \ldots & c(0,0)+N & c(x_{n0},t) & 1 \\ c(x_{10},t) & c(x_{20},t) & \ldots & c(x_{n0},t) & c(0,0)+N & 1 \\ 1 & 1 & \ldots & 1 & 1 & 0 \end{pmatrix} \cdot \begin{pmatrix} w_1 \\ w_2 \\ \vdots \\ w_n \\ v \\ \lambda \end{pmatrix} = \begin{pmatrix} c(x_{01},0) \\ c(x_{02},0) \\ \vdots \\ c(x_{0n},0) \\ c(0,t) \\ 1 \end{pmatrix}, \tag{10}$$

where x_{ij} denotes the distance between locations p_i and p_j, and $t=|t_M-t_G|$ the time difference between MERIS and GPS time. N is the nugget. The VC-matrix on the left in Eq. (10) contains the spatially varying covariances $c(x_{ij},0)$ between the GPS IWV observations in the $n\times n$ top left part. Row and column (n+1) contain the spatio-temporal covariances $c(x_{i0},t)$ between the MERIS observation and the n GPS observations, while the last row and column ensure an unbiased prediction. In the proximity vector on the righthand side, the first n entries contain the spatially varying correlations $c(x_{0i},0)$ between the prediction location and the locations of the GPS IWV observations. The $(n+1)$-th entry c(0,t) gives the time-

dependent covariance between MERIS observation $I_M(p_0, t_M)$ and the collocated prediction location[c1], while the last entry again is obtained from the unbiasedness condition $w_1 + \cdots + w_n + v = 1$. The additional nugget, N, on the diagonal of the VC-matrix expresses the uncertainty in the IWV observations. Omitting the nugget in the proximity vector at space-time coincidence of an observation with the prediction is important, because in this case the Kriging system will not simply return the observation as prediction at such a coincidence, a property generally referred to as *exactness*, but will rather divide weight over nearby observations as well, which also results in a more realistic residual error variance value.[a2] Solving Eq. (10) gives a unique solution for the weights, due to the positive definiteness of the VC-matrix.

Except for an IWV prediction $\hat{I}(t_G, p_0)$ we obtain a quality description in the form of a residual variance $\mathrm{var}(r_0)$, with $r_0 = \hat{I}(t_G, p_0) - I(t_G, p_0)$ the difference between the prediction $\hat{I}(t_G, p_0)$ and the (unknown) real value $I(t_G, p_0)$ of the IWV at the prediction space-time point, cf. (Goovaerts, 1997; Wackernagel, 2003). The residual variance is given by

$$\mathrm{var}(r_0)_{(t_G, p_0)} \;=\; c(0,0) - \sum_{i=1}^{n} w_i \cdot c(x_{0i}, 0) - v \cdot c(0,t) - \lambda \tag{12}$$

Basically, the residual variance expresses the proximity, both in space and time, of the observations to the prediction point. The residual variance is minimal at the GPS IWV observation locations and at MERIS acquisition times while it increases with increasing distance, in space and time, between the prediction location and observation locations until no correlation with any of the observations remains. This is illustrated in Fig. 2 where the mean, minimum, and maximum residual variances per epoch of IWV

[c1] *changed from:*

$$\begin{pmatrix} 1 & \mathrm{cs}_{12} & \dots & \mathrm{cs}_{1n} & 0 & 1 \\ \mathrm{cs}_{21} & 1 & \dots & \mathrm{cs}_{2n} & 0 & 1 \\ \vdots & \vdots & \ddots & \vdots & \vdots & \vdots \\ \mathrm{cs}_{1n} & \mathrm{cs}_{n2} & \dots & 1 & 0 & 1 \\ 0 & 0 & \dots & 0 & 1 & 1 \\ 1 & 1 & \dots & 1 & 1 & 0 \end{pmatrix} \cdot \begin{pmatrix} w_1 \\ w_2 \\ \vdots \\ w_n \\ v \\ \lambda \end{pmatrix} = \begin{pmatrix} \mathrm{cs}_{01} \\ \mathrm{cs}_{02} \\ \vdots \\ \mathrm{cs}_{0n} \\ \mathrm{ct}_{0M} \\ 1 \end{pmatrix} \tag{11}$$

The VC-matrix on the left in Equation 10 contains the spatial correlations cs_{ij} between the IWV-GPS observations in the $n \times n$ top left part. The $n+1$-th row and column express that no correlation is assumed between the spatial and temporal contributions to the system, while the last row and column are added for obtaining an unbiased prediction. In the proximity vector on the right, the first n entries contain the spatial correlations cs_{0i} between the prediction location and the locations of the GPS-IWV observations. The $(n+1)$-th entry ct_{0M} gives the temporal correlation between the prediction time, t_0, and the MERIS-IWV observation time, t_M

[a2] *new text added*

estimates are given, based on both GPS and MERIS IWV observations. The minimum variance is almost stable at a level of 10 kg/m^2, reflecting that in each epoch some prediction locations are in the direct vicinity of GPS observations. The mean and maximum variance decreases around the MERIS acquisition time around 10:15 AM to increase again after that. If another MERIS snapshot would be available at, say, 8 PM, again the mean and maximum variance would decrease around that time.[c1]

The data fusion procedure as described here is a collocated approach because only the MERIS IWV pixel at the prediction location is taken as an observation. It is fast as the size of the linear system Eq. (10) is small. The size depends only on the number of GPS ground stations. When interpolating to a map at given GPS epoch time t_G, only the one collocated MERIS observation $I(t_M, p_0)$ changes with the prediction location p_0. Therefore only the covariances in row and column $(n+1)$ of the VC-matrix and the first n entries in the proximity vector need to be updated. Disadvantage of such collocated method is that it will not fill any spatial gaps in the MERIS grid. This could be resolved by including a spatial interpolation component for the MERIS observations as well, at the expense of computational efficiency.[c1]

4 Data description, comparison and combination.

The position of all data considered here is given in WGS84 (World Geodetic System 1984) coordinates. Spherical distances between points are computed along great circles with respect to the WGS ellpisoid. Time is given in Coordinated Universal Time (UTC).[c2]

[c1] *changed from:* to the observations. It is locally minimal at the GPS IWV observation locations and at MERIS observation time while it increases together with the decrease in correlation between the prediction space-time point and the observations.

[c1] *changed from:* This approach is known as the collocated approach. It is fast as the linear system in Eq. (10) is small. The size depends only on the number of GPS ground stations. Moreover the VC-matrix is fixed during the interpolation, which implies that it only needs to be inverted once. The values in the proximity vector however are different for each prediction space-time point. Disadvantage of this method is that it will not fill any spatial gaps in the MERIS grid. This could be resolved for by including a spatial interpolation component for the MERIS observations as well, but then the computational efficiency will be lost.

[c2] *changed from:* that is, the position of a data point is given by a latitude and a longitude with respect to the WGS84 reference ellipsoid. Distances between points are spheroidal and are computed along approximate great circles with respect to this ellipsoid. Time is given in Coordinated Universal Time (UTC), which corresponds to the time zone of Greenwich on the western part of the scene considered.

4.1 *GPS IWV data description.*

The GPS data originates from the 26 GPS COST-716 ground stations, (Elgered et al., 2005), as shown in Fig. 3. We used as much data as possible from one processing center, therefore 24 stations were taken from the GeoForschungsZentrum (GFZ) in Potsdam. Two additional stations processed by the Nordic Geodetic Commission (NKG), were added to improve the spatial coverage. For the given list of stations we consider all available IWV data from August 9, 2003. For the GFZ stations most IWV estimates are available at h:15 and h:45, where h indicates the integer hours, but some data are missing. NKG data is available at 15 minute intervals, but here data points are missing as well.

4.2 *MERIS IWV data description.*[c1]

We used one MERIS reduced resolution product, acquired at August 9, 2003, between 10:11:27 and 10:14:44 UTC. At reduced resolution, one pixel is available for every 1.2×1.2 km^2 at nadir direction. The MERIS reduced spatial resolution of 1.2 km is much higher than the approximate spatial resolution of 50 km of the GPS IWV estimates at ground stations. Therefore, the reduced MERIS IWV product is suitable to demonstrate the advantages of combining GPS and MERIS IWV data. Further improvements are expected with full resolution (300 m) MERIS IWV data[a2]

Data flags. A MERIS Level 2 data set contains an *Integrated Water Vapor* attribute. The value of this attribute at a given position may not always be representing the actual IWV value, due to e.g. the presence of cloud cover. Therefore a filter step is necessary. Except for several data attributes, the MERIS Level 2 product also provides a quality attribute by assigning binary 24-bit flags to each product pixel. A unique combination of zeroes and ones addresses the pixel state and quality, according to the classification of the MERIS pixels.

We removed IWV points for which the CLOUD flag, the PCD_14 flag, or the TOAVI_CSI flag is true, see Fig. 4. The CLOUD flag indicates that the cloud product is available; the PCD_14 flag indicates that

[c1] *changed from:* Processing the MERIS data.
[a2] *new text added*

the total water vapor content is uncertain, while the TOAVI_CSI flag indicates cloud, snow or ice over land pixels. For our test data set this filter step reduces the number of points in the scene by 20% from 1.25 to 1.09 million points. The other flags were ignored.

4.3 *GPS and MERIS IWV*[a1] *comparison at MERIS time.*

Single pixel comparison. After filtering the MERIS data[c2], a comparison was made between the GPS IWV values at the MERIS acquisition time and the values of the remaining MERIS pixels close to the GPS stations. First the MERIS pixel nearest[c3] to each of the GPS stations was determined, see Fig. 5. The correlation between these GPS and MERIS estimates is only 0.63. This relatively low correlation value is mainly caused by some strong outliers. Especially near Stavanger (STAS), Oberpfaffenhofen (OBE2), Pfaender (PFAN) and, to a lesser degree, near Braunschweig (PTBB) and Helgoland (HELG), agreement in estimates is poor. Therefore the MERIS pixels around these GPS stations were considered in detail. In Fig. 6 the values of the 25 MERIS pixels closest to four such GPS stations are shown: PFAN, HELG, PTBB and STAS.[c4] The situation around GPS station OBE2 is not considered, as the nearest MERIS pixel is at a distance of more than 10 km. Around three stations we observe big discrepancies between neighboring MERIS pixels: in all three cases jumps of more than 5 kg/m^2 exist. Around STAS a jump from 25.8 kg/m^2 to 49.8 kg/m^2 occurs. An explanation for these jumps can be found in the MERIS flags.

Near the PTBB station two single flags, the 'LAND' flag and the 'PCD_19', an aerosol related confidence flag, are true for all pixels and those pixels all have similar values. Around HELG we see more variability in the MERIS pixel values, and in the flags as well. In this case however pixels with similar values not necessarily have identical flags. What should be noted here is that all pixels are marked as 'water', so the existence of the two small islands of in total 1.7 km^2 that form Helgoland cannot be recognized on the MERIS image.

Around PFAN we find both 'LAND' and 'WATER' pixels. All MERIS pixels with relative high values are

[a1] *new text added*
[c2] *changed from:* removal of suspicious MERIS points
[c3] *changed from:* closest
[c4] *changed from:* In Fig. 6 the values of 25 MERIS pixels are show around four GPS stations with values deviating from the nearby pixel values.

'LAND' pixels. Intermediate values are found at 'LAND' pixels that are marked as 'COASTLINE' pixels as well. Around STAS the situation is reversed. Here the 'WATER' pixels have high values compared to the 'LAND' pixels. Both in the PFAN and the STAS case the values of the 'LAND' pixels are nearest to the IWV value as determined by the nearby GPS station.

All encountered problems occurred for stations situated near land-water boundaries. Strong jumps in MERIS IWV estimates were observed between neighboring pixels, partly due to different IWV estimations methods used over land and water. Moreover, MERIS pixels exist, e.g. near Helgoland, that are classified as water, although they clearly contain a land component.[a1]

Correlation MERIS-GPS vs. GPS area of influence size. After determining the correlation for different AOI sizes of the GPS estimates, as described in Section 2.2, it is found that the maximum correlation occurs for $R_{\mathrm{GPS}} = 1.75$ km. For this AOI of about 10 km^2 the GPS-MERIS correlation equals 0.79. Using this radius implies that about 8 MERIS pixels closest to a GPS station are used in the correlation comparison. Note that indeed a maximum in correlation is found inside the interval between 0 km and the upper bound of $R_U =$ 58[c2] km, as derived in Section 1.

We discard stations with a maximal absolute difference of more than 5 kg/m^2 between the MERIS pixels within the GPS AOI. In this way the stations of ONSA, PFAN, STAS and TERS (all coastal!) are removed from the comparison because of big jumps, while DELF and OBE2 have no MERIS data to compare within the GPS AOI. For the remaining stations we find a RMS difference of 2.3 kg/m^2, which is comparable to the reported accuracies of the GPS and MERIS IWV observations. A regression analysis yields a Pearson correlation coefficient of 0.85.[c3]

[a1] *new text added*
[c2] *changed from:* 15
[c3] *changed from:* A correlation of 0.853 is obtained if stations are discarded[c4] with a maximal difference of more than 5 kg/m^2 between the MERIS pixels within the GPS footprint. In this way the stations of ONSA, PFAN, STAS and TERS (all coastal!) are removed from the comparison because of big jumps, while DELF and OBE2 have no MERIS data to compare within the GPS footprint.

4.4 *Experimental spatial and temporal covariance analysis*[c5]

GPS spatial correlation As only 26 GPS stations are considered, it is difficult to determine a reliable covariogram for the spatial correlation at a single epoch. Therefore a spatial experimental covariogram is determined from the, if necessary, linearly interpolated GPS measurements at every hour between 0.30 and 23.30. These times are chosen because most IWV estimates are available at exactly the half hours. The covariogram for 10:30 is shown in dark blue in Fig. 7a. For the hourly covariograms only those interpolated GPS IWV values are used for which at least one measurement is available within one hour of the covariogram time. The mean of the experimental covariograms obtained in this way is shown in red in Fig. 7a. This covariogram displays a range, i.e. the maximum distance at which correlation exists, of about 200 km, which agrees for all individual covariograms. The sill or, more precisely, the average experimental covariance within the first bin of 60 km of the individual covariograms, is highly variable during the day, and is on average about 50 $(kg/m^2)^2$.[c6] This shows that the size of the spatial covariance of the IWV signal as measured by GPS is highly variable with time, although its[c7] range seems more stable. [r8]

MERIS spatial correlation The experimental covariogram of a subset of about 1100 MERIS IWV observations is represented by the dotted line in Fig. 7a. Here a bin width of 10 km is used. This covariogram is fairly comparable to the covariogram of the GPS IWV data at 10:30. Due to the higher spatial resolution, the range of the MERIS covariogram is higher than the GPS range and is equal to almost 500 km.

GPS temporal correlation The time series of the GPS IWV at the different GPS ground stations display a strong trend. To ensure second order stationarity[a1], a linear trend was fitted at each station and removed from the data. The mean of the 26 temporal covariance functions determined from the detrended data is given by the brown dots in Fig. 7b. As the IWV values at most stations even show some non-linear trend

[c5] *changed from:* Data correlation.
[c6] *changed from:* and varies from 40 at 00:30 downwards to -10 at 06:30 and then again upwards via 50 at 10:30 (figure) up to 90 at 15:30, in order to end at 23:30 at a value of 65.
[c7] *changed from:* it's
[r8] *removed:* A more elaborated approach can be found in (de Haan et al., 2005).
[a1] *new text added*

during the day, the stationarity condition for an underlying random function does not hold very well. This is expressed by the negative covariance values at higher distances. From the figure it is concluded that the temporal covariance stabilizes after about 10 hours.[a2]

4.5 *Optimizing the GPS IWV prediction.*

When producing IWV maps from GPS IWV observations, MERIS observations can be used in two different ways. First, MERIS observations can be directly incorporated to produce the water vapor maps as as sketched in Section 3.2. For this purpose a spatio-temporal covariance function as in Eq. (8) needs to be determined.[c1] Second, the MERIS IWV observations can be used to validate the covariance parameters of the GPS IWV observations.

In order to setup a MERIS reference image, needed for validation of the GPS IWV interpolation, the MERIS observations are resampled to a 0.25×0.1 degree longitude-latitude grid. This implies that one grid cell has an approximate size of 17×11 km. The cell size is small enough to represent local variations in the MERIS signal, and large enough to ensure computational efficiency.[c2]

In the following, the resampled MERIS data are used as reference data for optimizing parameters for the interpolation of the GPS IWV data near MERIS time. As a benchmark, the mean absolute difference between the gridded MERIS data and the mean of the GPS IWV observations equals 4.57 kg/m^2. Two methods are used for interpolation of the GPS IWV data. For both methods optimal parameter values were determined by minimizing the mean absolute difference at the 0.25×0.1 degree lon-lat grid between the resampled MERIS and the interpolated GPS IWV values. First, the GPS IWV observations were interpolated using inverse distance weighting, that is, a weight w_j is assigned to each observation, according

[a2] *new text added*

[c1] *changed from:* Cokriging approach as sketched above. For this purpose the individual VC-matrices of both the GPS and the MERIS observations are needed together with the cross-correlation VC-matrix containing the cross-covariances between the MERIS and GPS observations.

[c2] *changed from:* Moreover, the MERIS IWV observations can be used to gauge and control the covariance parameters of the GPS IWV observations. For this purpose the MERIS observations are gridded to a 0.25×0.1 degree longitude-latitude grid. This implies that one grid cell has an approximate size of 17×11 km. The cell size is chosen such that local variations in the MERIS signal are still representable, while the size is not so small that computations become too time consuming. The gridding is done by identifying the nearest neighbor in each of the eight octants around a grid-point and combining these eight points to an interpolated value by means of a quadratic inverse distance scheme. Note that in comparison to Fig. 3 all smaller gaps have been filled. Grid points for which no observation is available in all eight octants within 100 km did not get a value.

to

$$w_j(p) = \frac{1}{\sum_{i=1}^{n}(1/d_i^p)} \cdot \frac{1}{d_j^p}, \tag{13}$$

where n denotes the number of observations and d_j the spherical distance between the interpolation location and the observation. Here the only parameter to determine is the power p of the interpolation. The mean absolute difference reaches its minimum value of 4.06 for $p = 3$. The mean absolute difference is determined for different parameters settings within the ordinary Kriging framework as well. Here a minimum absolute difference of 3.90 was obtained with a nugget of zero, a sill of 10, and a range of 3000 km, while using the exponential model. The result of the GPS IWV interpolation using these settings is shown in Fig. 8b, while Fig. 8c shows the difference between the resampled MERIS data and the resulting GPS map.

It is remarkable that the experimental covariance functions as derived in Section 4.4 indicate a much shorter range [r1] than found by the optimization procedure described here. The reason is the often large distance between the interpolation locations and the nearest observations. In such case, ordinary Kriging will not assign a higher weight to the most close observations as these are still beyond the correlation range.[c2] As a result, the prediction value will be close to the Kriged mean, that is, the mean which incorporates the correlation between the observations. Due to the use of a long range the Kriging system assigns a higher weight to the nearest observation which leads to better results in the comparison with the MERIS data.

[r3]

Comparing GPS and MERIS IWV maps. In Figure 8 we see MERIS, Fig. 8a, and GPS, Fig. 8b, observations interpolated to the same grid at MERIS acquisition time. Clearly, in the MERIS data, small

[r1] *removed:* of 200 km from just the GPS IWV data and still only 500 km from the MERIS IWV data

[c2] *changed from:* Indeed, a range of 500 km, together with a sill of 50 and a filtered nugget of 1, while still using the exponential model, results in a mean absolute difference of 4.097. The need for using a long range is caused by the often large distances between the interpolation locations and the observations. When using a short range, the ordinary Kriging system will not assign higher weights to the nearest observations, as according to the range there is no correlation between the prediction location and the observations.

[r3] *removed:* In Figure fdiff, a difference plot is given between the optimal map as obtained by ordinary Kriging (OK) and by Inverse Distance. For blue points Inverse Distance gives a higher prediction, whereas for red points ordinary Kriging gives higher values. The differences can be explained by the clustering and screening properties of OK as discussed in Section 6. In the middle of the picture for example OK gives a higher prediction value. This is because the lower observation values in the west of The Netherlands and in Belgium are screened off by the higher values at EUSK and WSRA.

scale features of IWV distribution are preserved that are not visible in the interpolated GPS image. It is apparent that the low resolution GPS observations cannot detect fine IWV structure in the spatial domain. This shows the relevance of the use of additional information about spatial IWV distribution, as provided e.g. by MERIS observations.[a4] In the difference picture, Fig. 8c, green indicates areas for which IWV values are underestimated by the GPS interpolation. In contrary, red indicates areas of overestimation. This figure clearly demonstrates the amount of information that is missed when only using GPS IWV estimates.[c5]

4.6 *Spatio-temporal combination.*

In this paragraph a first result of the spatio-temporal interpolation procedure as described in Section 3.2 is presented. In order to produce realistic residual variances of the spatio-temporal estimates, the parameter settings as derived from the spatio-temporal experimental covariance analysis of above are adapted. The common spatio-temporal sill is set to 50 $(kg/m^2)^2$. The common spatio-temporal nugget value of 3 $(kg/m^2)^2$ reflects the reported GPS and MERIS IWV standard deviations, cf. Section 2, of 1-2.5 kg/m^2. The spatial covariances are taken from an exponentially decreasing model with a range of 500 km. The temporal covariance is modeled by a spherical function with a range of 10 hours.[a1]

In Figure 9 three epochs of IWV estimates, a)-c), together with their variances, d)-f), are shown. Figures 9a and 9d give the estimates and their variances at 10:30 UTC, close to MERIS IWV observation time. Here many small-scale details are visible, having the same pattern as in Figure 3, which shows the MERIS IWV observations alone. Nevertheless, it is clear to see that the small-scale details are less profound in the combined estimation map. The variances are low, about 10 $(kg/m^2)^2$ and homogeneous, as for every estimation location a nearby MERIS IWV observation exists. Figures 9b and 9e give the estimates and their variances at 13:30 UTC. Here the GPS IWV observations are dominant at locations where the GPS

[a4] *new text added*

[c5] *changed from:* This figure shows that even the (higher) OK interpolated GPS IWV values underestimate the MERIS observations. which shows that in this case the OK estimates are closer to the MERIS values as the Inverse Distance estimates. We conclude that for interpolation of the GPS IWV stations OK gives the best result. As the number of stations is limited, using OK is also feasible from a computational point of view: the variance-covariance matrix of the pair-wise correlations between the observations that has to be inverted, is small

[a1] *new text added*

ground station configuration is more dense, while smaller scale details are visible in regions with sparse GPS information, for example west of Norway. The error variances clearly reflect the availability of the GPS observations: around the GPS stations the variance is minimal and increases with increasing distance to the nearest GPS station until a maximum of about 40 $(\mathrm{kg/m^2})^2$ is reached. At 18:30 the predicted IWV distribution, Figure 9c, is very smooth because it is by now completely driven by the GPS IWV observations, as there is no temporal correlation anymore with the MERIS acquisition.[c2]

The variances, Fig. 9f, show the same pattern as at 13:30 UTC, but are larger, especially in regions further away from the GPS stations, as the lack of temporal correlation with the MERIS image is the most influential on the variance at locations where also the spatial correlation with the GPS observations is low. Note that an overview of the development of the minimum, mean and maximum error variances during the day is already given in Fig. 2. The variance maps clearly show that acceptable combined spatio-temporal estimations can only be achieved when the spatio-temporal availability of GPS and MERIS IWV estimates is good enough. As only a part of the operational GPS ground stations were used in this research, the optimal possible situation, especially over European land area, is much better than demonstrated here.[c1]

5 Conclusions and further research.

In this paper we present the results of a spatio-temporal combination of GPS and MERIS IWV observations. The combination is performed by solving an ordinary Kriging system with suitable spatio-temporal covariances between MERIS and GPS measurements. For this purpose we used GPS IWV data from 26 GPS ground stations and a MERIS image acquired at a nearly cloudless day in 2003. As a first step GPS and MERIS IWV data from the same time and location were compared in order to assess the consistency

[c2] *changed from:* In Figure 9, some results of the spatio-temporal interpolation procedure as described in Section 3.2 are shown. The left most figure gives the prediction at 10:30, close to MERIS-IWV observation time. Here a lot of small-scale detail is visible, in the same pattern as in Figure 3, that showed the MERIS-IWV observation alone. The combination with the GPS-IWV observations reduces the size of local deviations that are only present in the MERIS-IWV observations however. The middle figure gives a prediction for 14:30 and here the GPS-IWV observations are dominating, but still some smaller scale details are visible, for example off the Norway cost, that were only present in the MERIS-IWV data set. At 18:30 the prediction map is very smooth because it is by now completely dominated by the GPS-IWV observations as there is no temporal correlation anymore with the MERIS acquisition time. The same kind of change in pattern is observed in the prediction map produced for time points before MERIS-IWV acquisition time.

[c1] *changed from:* What remains is to give a good quality description of the IWV predictions obtained in this way. As discussed in Section 3.2, the Kriging error variance gives an indication for the proximity of the observation points. A step that still has to be added however, is to incorporate the drift of the water vapor field due to wind power into the spatio-temporal interpolation procedure. This step, combined with a validation step using e.g. a one month time series of both GPS IWV and MERIS IWV data sets can lead to an adequate quality description of the combined MERIS-GPS water vapor product.

of the IWV estimates from both the systems.[c2]

We found a correlation of 0.85 and a RMS difference of 2.3 kg/m^2 when comparing an IWV observation at a GPS station with the average of the MERIS IWV pixels within a circle with optimal radius of 1.75 km. Coastal stations with a jump between neighboring MERIS IWV pixel values of more than 5 kg/m^2 within the GPS area of influence were removed. Such jumps, far beyond the specified accuracy, typically occurred near coastline GPS stations, because the MERIS IWV algorithm uses different methods above land and water. A further analysis of near-coastal IWV values may lead to an improvement of the current algorithms as used by MERIS for processing IWV data. The resulting correlation value shows that the reported accuracies of the MERIS and GPS IWV observations are consistent.

The spatially dense MERIS IWV observations can be used as reference data to find optimal parameter values for the spatial interpolation of the GPS IWV observations. In this way a much longer correlation range is found than that provided by the experimental covariance function analysis. The first results of a spatio-temporal combination of the GPS and MERIS IWV observations match the intuition. Moreover, the estimated residual error variances give a quality description of the combined IWV product at a given time and location. One known problem with this type of variance however is that it only depends on data configuration rather than on data values. In case of pixel jumps, one might obtain too optimistic variance estimates. An alternative approach for assessing local uncertainty is to simulate many possible realizations of the IWV distribution and to consider the variability in the outcomes at a given time and location, (Goovaerts, 1997). This computationally more elaborated approach is expected to provide realistic variance estimates, even in case of jumps.[a1]

A next step of this research will be to incorporate wind data in the spatio-temporal combination, as, according to Taylors frozen flow assumption, wind transports water vapor fields as a whole, albeit to a limited temporal extent.

Another necessary extension, especially when considering IWV estimates over mountainous areas, is to include topographic height information in the spatio-temporal interpolation of the GPS and MERIS IWV

[c2] *changed from:* GPS and MERIS IWV observations are compared and combined.
[a1] *new text added*

observations. It is well-known that the IWV content decreases exponentially with increasing topographic elevation. Therefore, heights from a suitable digital elevation model, e.g. ESA's GETASSE30 30 arc second resolution product, (Brockmann et. al., 2006), should be incorporated in the interpolation. Two different procedures demonstrate such approach for the spatial interpolation of GPS IWV data alone, one over Switzerland, (Morland and Mätzler, 2005), where observations were normalized to a standard height of 500m, and one over Italy, (Basili et al., 2004), where heights were added to a Kriging system by means of a deterministic external drift.[a2]

The first results, as presented in this paper, were obtained with one day of observations only. Future research will focus on one month of consecutive MERIS IWV images together with high resolution GPS IWV time series. Testing data covering larger time intervals will allow for more adequate validation procedures. This will demonstrate the possible benefit from incorporating e.g. topography and wind information. Comparing predictions one hour ahead with real measurements will allow for better gauging of the spatio-temporal interpolation parameters. This will lead to an adequate quality description of the combined MERIS-GPS water vapor estimates. Given a sufficient number of GPS stations, this procedure will result in a high quality near real-time, spatially dense water vapor product to be used in numerical weather forecast models as well as in various applications using (In)SAR and GPS/Galileo.

Acknowledgments.

We would like to thank Sybren de Haan from the Dutch Royal Meteorological Society, KNMI for providing the authors with the GPS IWV data as well as for his useful comments. The MERIS data used in this paper are disseminated by the European Space Agency, ESA. This project is funded under number EO-085 by the Netherlands Institute for Space Research, SRON. Finally we would like to express our thanks to the three anonymous reviewers who provided us with many valuable comments and advice.[a1]

[a2] *new text added*
[a1] *new text added*

References

Basili, P., Bonafoni, S., Mattioli, V., Ciotti, P., and Pierdicca, N. 2004. Mapping the atmospheric water vapor by integrating microwave radiometer and GPS measurements. *IEEE Transactions on Geoscience and Remote Sensing 42,* 8, 1657–1665.

Bennartz, R. and Fischer, J. 2001. Retrieval of columnar water vapour over land from back-scattered solar radiation using the medium resolution imaging spectrometer (MERIS). *Remote Sensing of Environment 78*, 271–280.

Bevis, M., Businger, S., Herring, T., Rocken, C., Anthes, R., and Ware, R. 1992. GPS Meteorology: remote sensing of atmospheric water vapor using the global positioning system. *Journal of Geophysical Research 97,* D14, 15787–15801.

Brockmann et. al., C. 2006. BEAM Version 3.6 - The Basic ENVISAT Toolbox for MERIS, (A)ATSR and ASAR. http://www.brockmann-consult.de/beam, Last visited: January 16, 2007.

Cess, R. D. 2005. Water Vapor Feedback in Climate Models. *Science 310,* 5749, 795–796.

Chilès, J.-P. and Delfiner, P. 1999. *Geostatistics: modeling spatial uncertainty.* Wiley Series in Probability and Statistics. John Wiley & Sons, New York.

de Haan, S., van der Marel, H., Gündlich, B., and Barlag, S. 2005. Resolving spatial and temporal atmospheric water vapour structures using a ground based GPS receiver network. Tech. Rep. project EO-050, SRON.

Elgered, G., Plag, H.-P., van der Marel, H., Barlag, S., and Nash, J. 2005. Exploitation of ground-based GPS for operational numerical weather prediction and climate applications, Final report. Tech. rep., COST Action 716, European cooperation in the field of scientific and technical research.

Fischer, J. and Bennartz, R. 1997. Retrieval of total water vapour content from MERIS measurements, Algorithm theoretical basis document. Tech. Rep. PO-TN-MEL-GS-0005, ESA-ESTEC, Noordwijk, Netherlands.

Gneiting, T., Genton, M. G., and Guttorp, P. 2007. Geostatistical space-time models, stationarity,

separability and full symmetry. In *Statistical Methods for Spatio-Temporal Systems*, B. Finkenstadt, L. Held, and V. Isham, Eds. Chapman & Hall/CRC, Boca Raton, 151–175.

Goovaerts, P. 1997. *Geostatistics for Natural Resources Evaluation.* Oxford University Press, New York, Oxford.

Hanssen, R. F. 2001. *Radar Interferometry.* Kluwer Academic Publishers, Dordrecht.

Hanssen, R. F., Weckwerth, T. M., Zebker, H. A., and Klees, R. 1999. High-Resolution Water Vapor Mapping from Interferometric Radar Measurements. *Science 283,* 5406, 1297–1299.

Jarlemark, P., Johansson, J., Stoew, B., and Elgered, G. 2002. Real time GPS data processing for regional atmospheric delay. *Geophysical Research Letters 29,* 16, 7/1–4.

Klein Baltink, H., van der Marel, H., and Van der Hoeven, A. G. A. 2002. Integrated atmospheric water vapor estimates from a regional GPS network. *Journal of Geophysical Research 107,* D3, 4025, doi:10.1029/2000JD000094.

Morland, J. and Mätzler, C. 2005. Spatial interpolation of GPS integrated water vapour measurements made in a mountainous terrain. Tech. rep., Institute of Applied Physics, Universität Bern.

Rothacher, M., Beutler, G., Brockmann, E., Fankhauser, S., Gurtner, W., Johnson, J., Mervart, L., Schaer, S., Springer, T., and Weber, R. 1996. The Bernese GPS Software Version 4.0. Tech. rep., Astronomical Institute, University of Berne, Switzerland.

Seemann, S. W., Li, J., Menzel, W. P., and Gumley, L. E. 2003. Operational Retrieval of Atmospheric Temperature, Moisture, and Ozone from MODIS Infrared Radiances. *Journal of Applied Meteorology 42*, 1072–1091.

Soden, B. J., Jackson, D. L., Ramaswamy, V., Schwarzkopf, M. D., and Huang, X. 2005. The Radiative Signature of Upper Tropospheric Moistening. *Science 310,* 5749, 841–844.

Taylor, G. I. 1938. The spectrum of turbulence. *Proceedings Royal Society London, Series A 164*, 476–490.

Thayer, G. 1974. An improved equation for the radio refractive index of air. *Radio Science 9*, 803–807.

Wackernagel, H. 2003. *Multivariate Geostatistics*, Third ed. Springer, Berlin.

Webb, F. and Zumberge, J. 1993. An introduction to GIPSY/OASIS-II. Tech. Rep. D-11088, Jet Propulsion Laboratory, Pasasena, California.

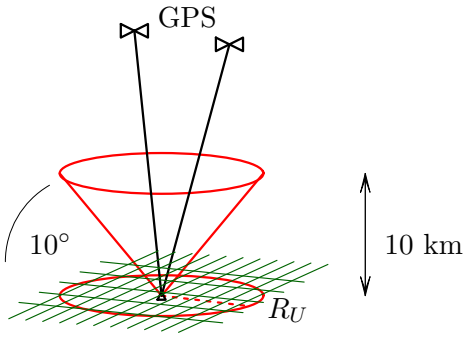

Figure 1. The projected circle indicates the upper bound for the GPS Area of Influence around the GPS ground station at the circle center, as derived from the cut off angle of 10 deg, combined with a tropospheric height of 10 km. The raster represents the MERIS pixels.

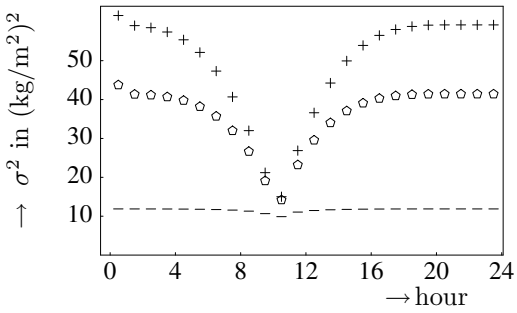

Figure 2. Minimum (dashes), mean (circles) and maximum (plusses) residual error variances per epoch of combined GPS and MERIS IWV estimates.

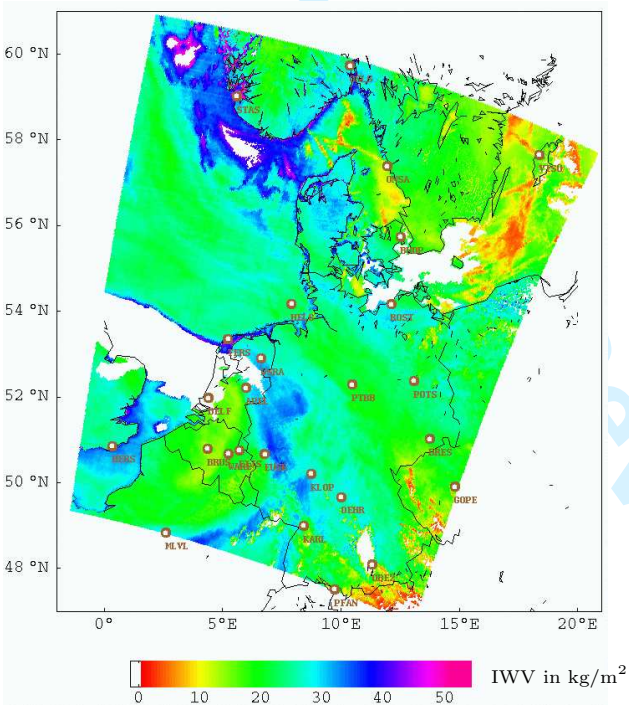

GPS Code	Site Name	Proc. center
APEL	Apeldoorn	GFZ
BRUS	Brussel	GFZ
BUDP	Kbenhavn	GFZ
DELF	Delft	GFZ
DRES	Dresden	GFZ
EIJS	Eijsden	GFZ
EUSK	Euskirchen	GFZ
GOPE	Pecny,Ondrejov	GFZ
HELG	Helgoland	GFZ
HERS	Herstmonceux	GFZ
KARL	Karlsruhe	GFZ
KLOP	Kloppenheim	GFZ
MLVL	Marne-La-Vallee	GFZ
OBE2	Oberpfaffenhofen	GFZ
ONSA	Onsala	GFZ
OEHR	Oehr	GFZ
OSLS	Oslo	NKG
PFAN	Pfaender	GFZ
POTS	Potsdam	GFZ
PTBB	Braunschweig	GFZ
ROST	Rostock-Warnemuende	GFZ
STAS	Stavanger	NKG
TERS	Terschelling	GFZ
VIS0	Visby	GFZ
WARE	Waremme	GFZ
WSRA	Westerbork	GFZ

Figure 3. MERIS water vapor data from August 9[c2], 2003, 10:15 UTC. The MERIS data will be compared and combined with water vapor data from the 26 indicated GPS ground stations.

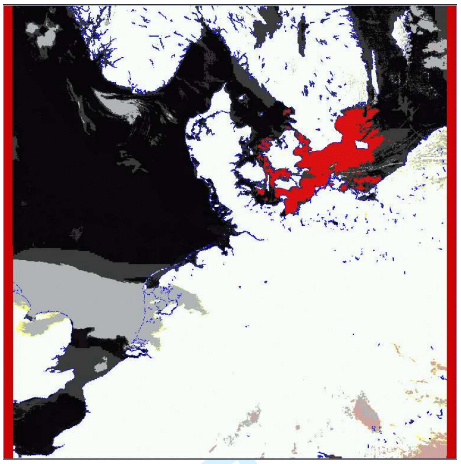

Figure 4. Classification according to MERIS flags. Clearly visible are the land (white), water (black) and coastline pixels (blue). 'Uncertain total water vapor content' is indicated in red, clouds in light gray and 'cloud, snow or ice over land' pixels are in yellow. These pixels were removed from the MERIS data set.

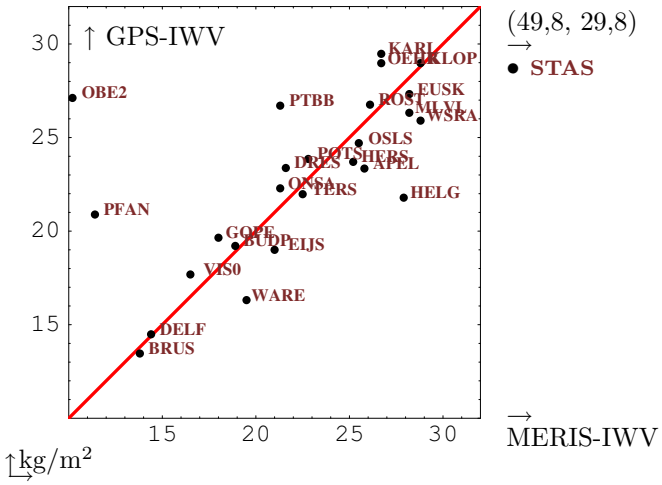

Figure 5. IWV values at GPS stations and at nearest MERIS pixel.

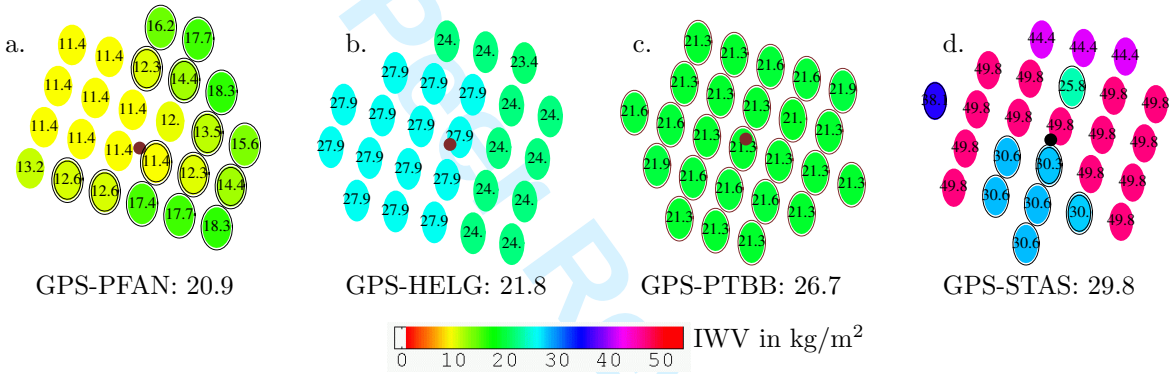

Figure 6. IWV values at 25 MERIS pixels nearest to a GPS station. a) Pfaender. b) Helgoland. c) Braunschweig. d) Stavanger. 'LAND' pixels are surrounded by one circle, 'COASTLINE' pixels by two circles.

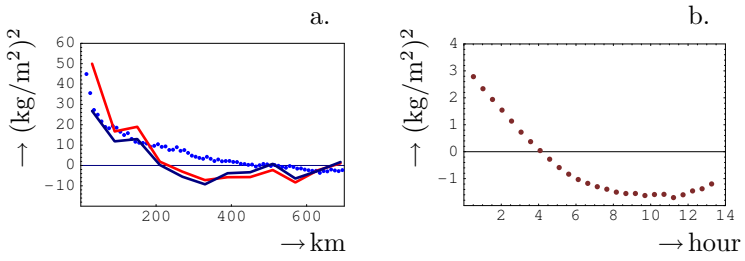

Figure 7. Covariograms of the IWV data. a) spatial. In dark blue: GPS covariogram at 10:30. In red: mean of 24 hourly spatial GPS covariograms. Dotted: covariogram of the MERIS data. b) temporal. Mean of the 26 temporal covariograms of the detrended IWV values at the different GPS stations.

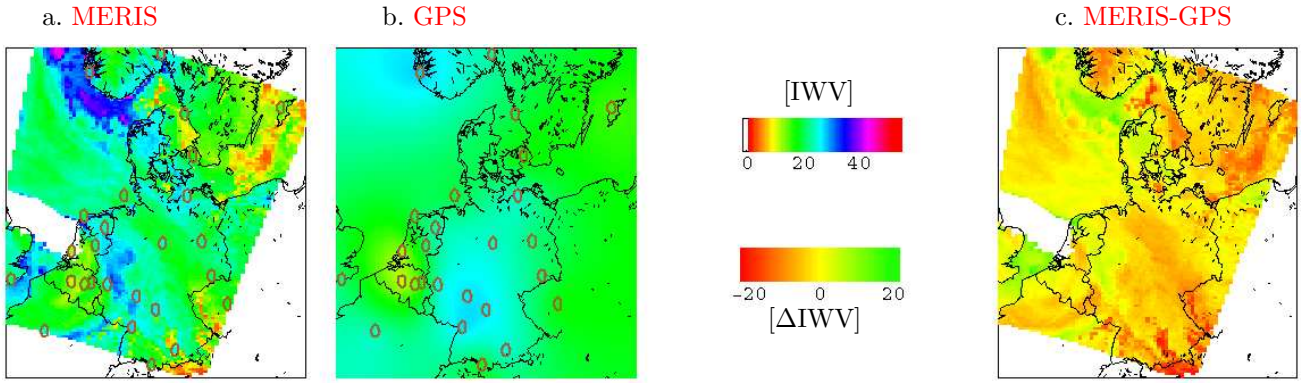

Figure 8. a) Resampled MERIS, and b) interpolated GPS IWV observations at MERIS time. Both data sets are on the same grid. c) shows the difference between a) and b).

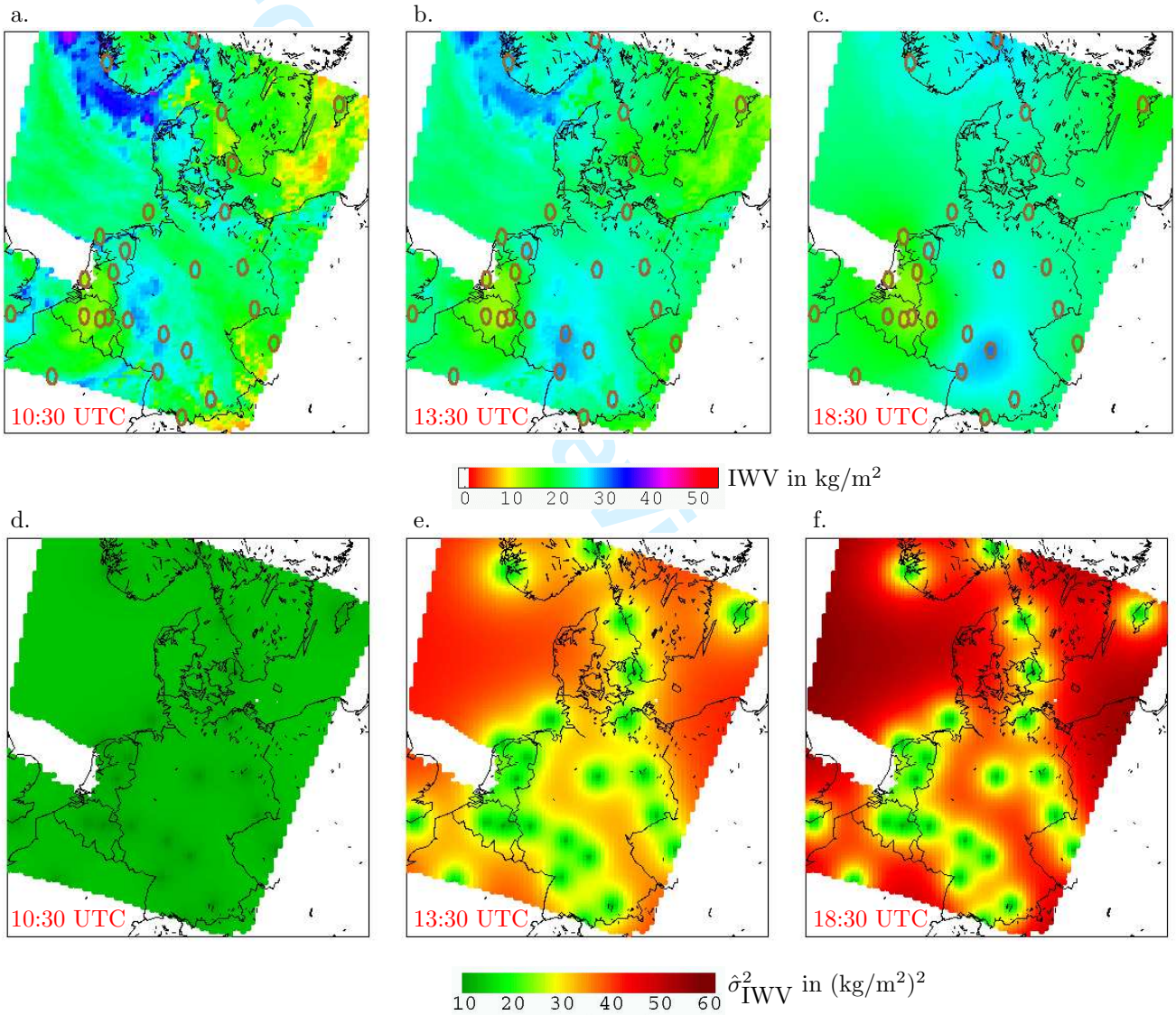

Figure 9. Top: maps of the IWV contents over North-West Europe at August 9[c3], 2003, a) at 10:30 UTC, b) at 13:30 UTC and c) at 18:30 UTC, obtained by combining IWV observations from MERIS and GPS. [n4] Bottom: residual variances of the IWV contents for a), b) and c) respectively.

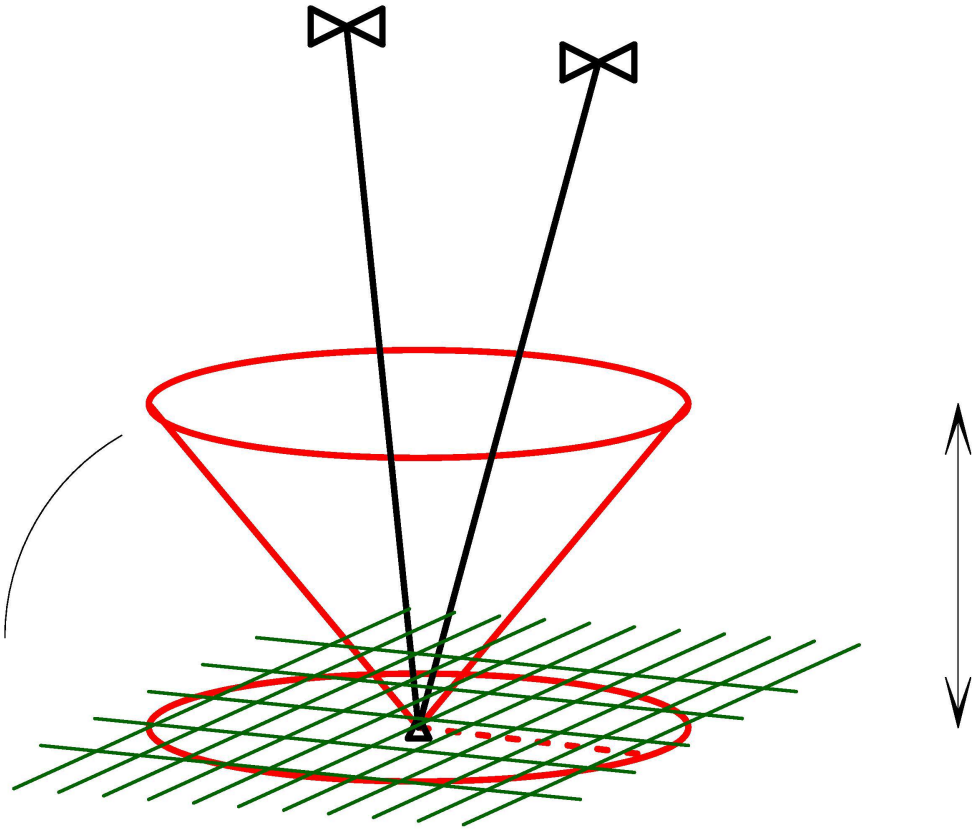

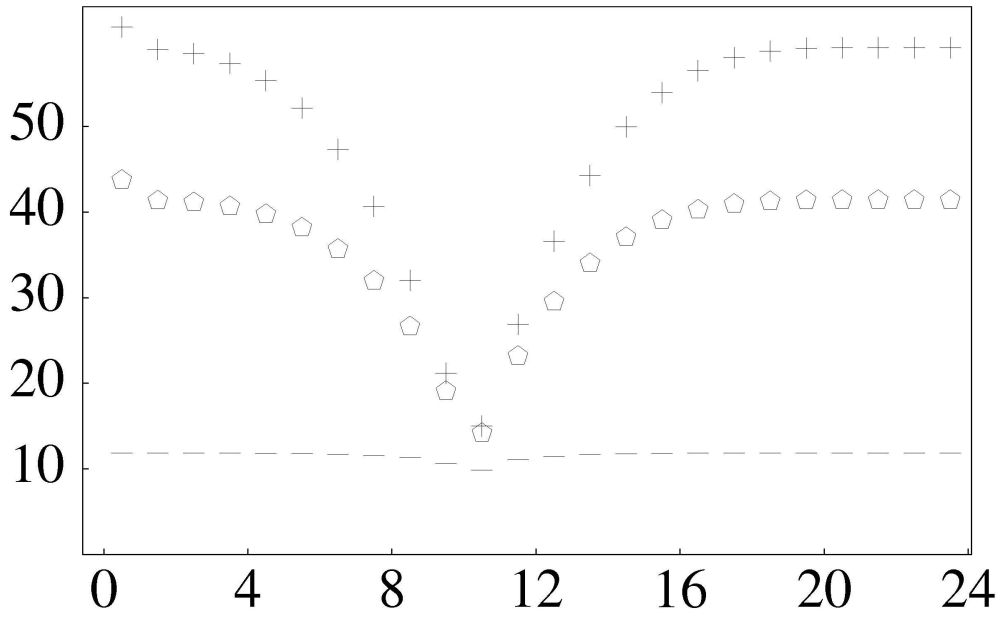

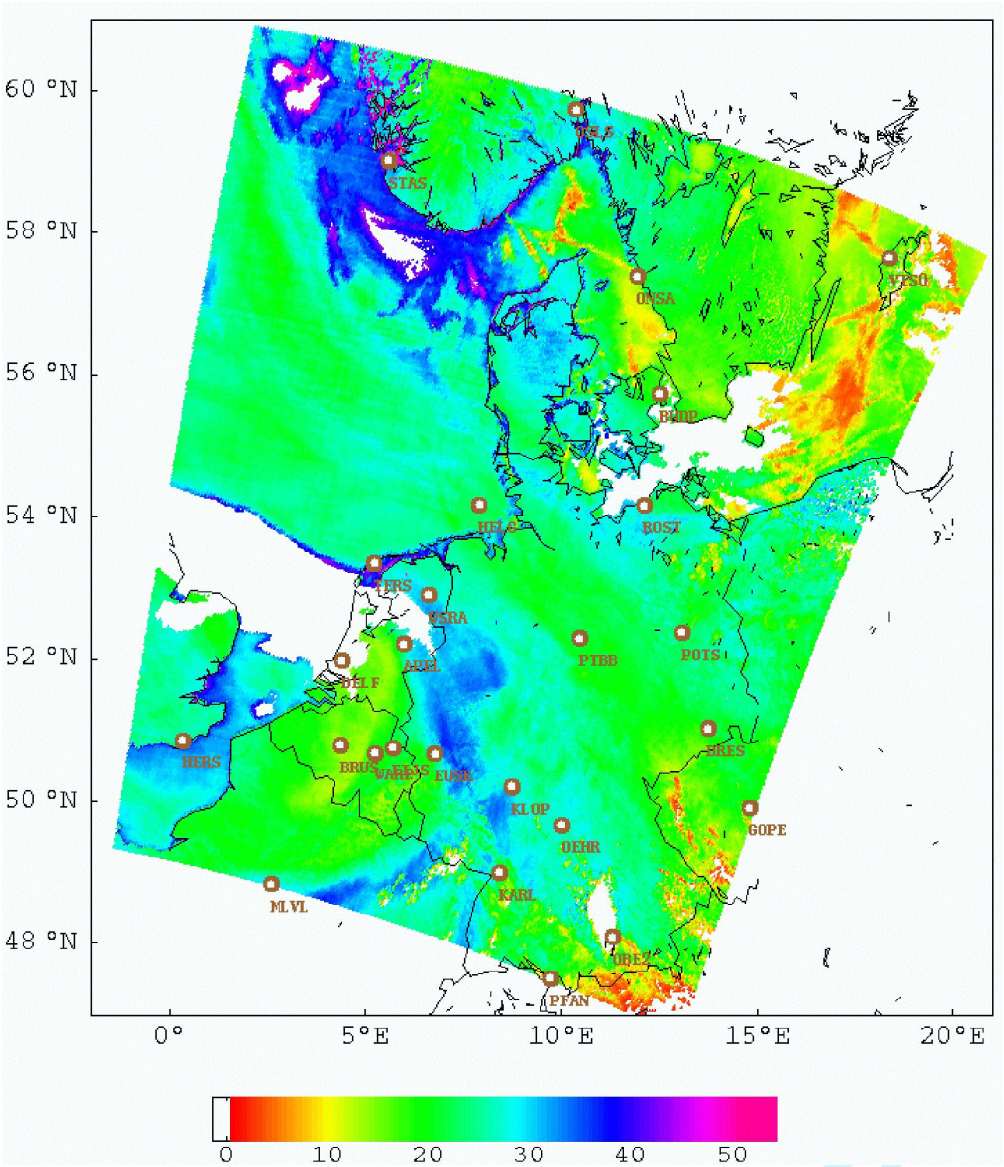
60 °N
58 °N
56 °N
54 °N
52 °N
50 °N
48 °N
0°
5°E
10°E
15°E
20°E
0
10
20
30
40
50
STAS
ESRA
AUEL
HERS
BRUS
KLOP
DEHR
KARL
MLVL
PTBB
POTS
HELA
ROST
GOPE
PFAN

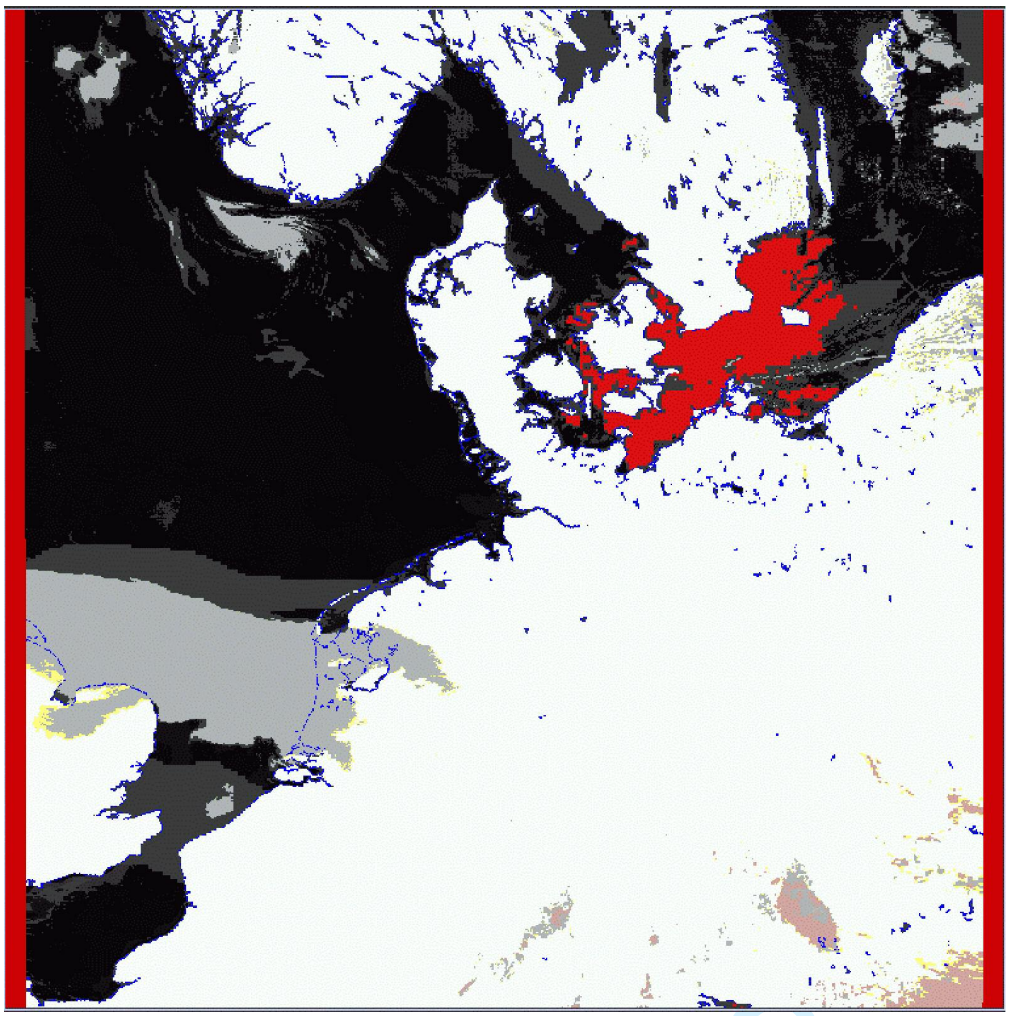

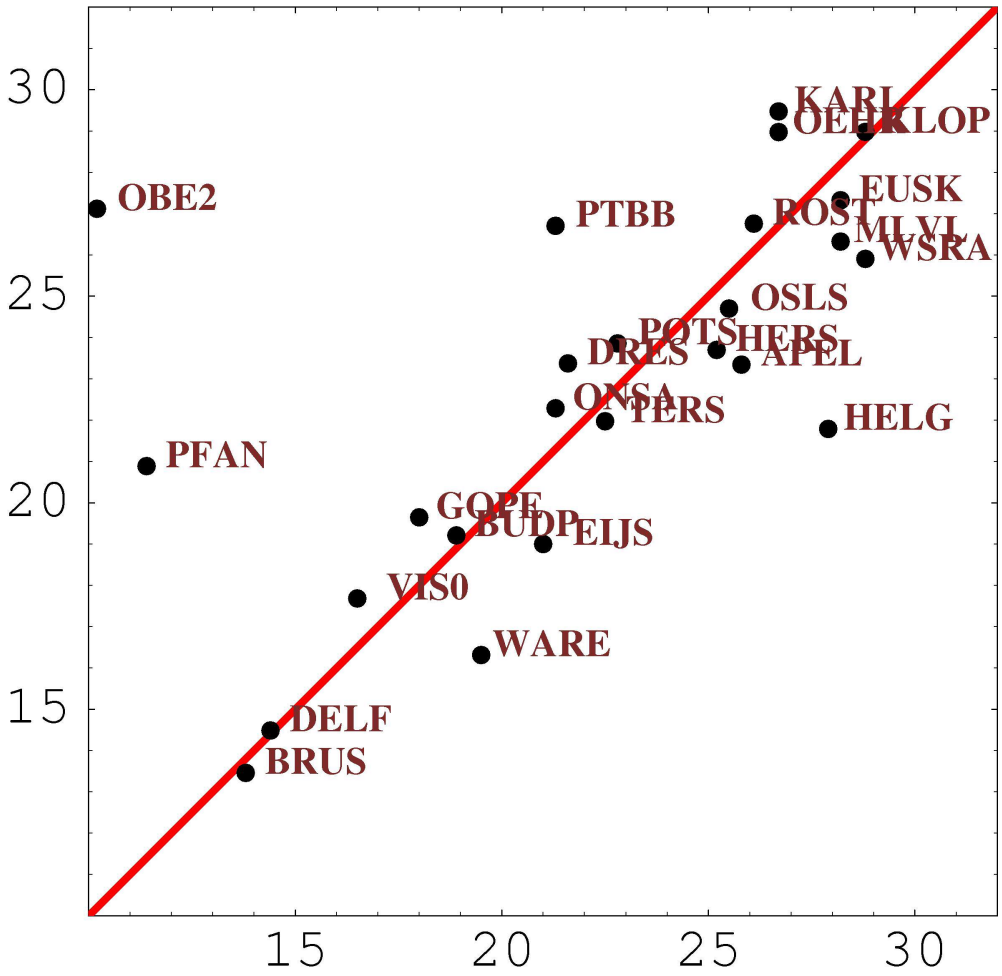

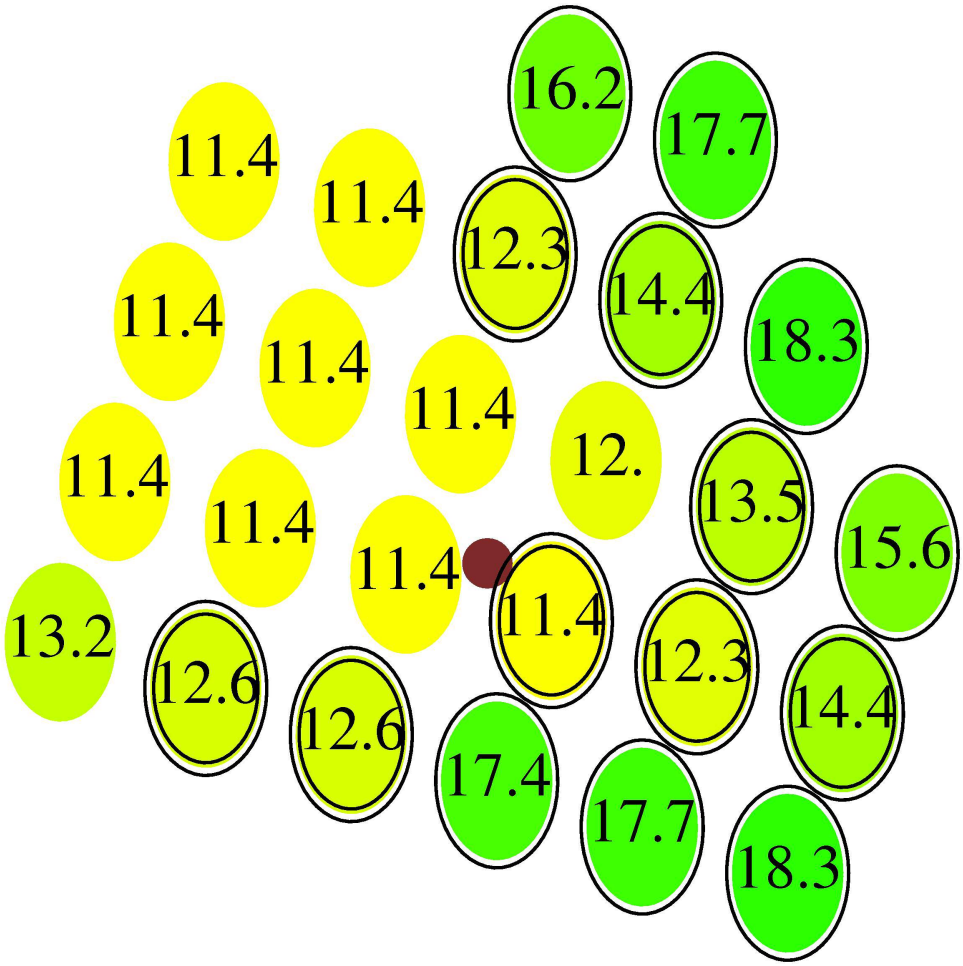
16.2
17.7
11.4
11.4
12.3
14.4
18.3
11.4
11.4
11.4
12.
11.4
13.5
15.6
11.4
11.4
11.4
11.4
13.2
12.6
12.6
12.3
14.4
17.4
17.7
18.3

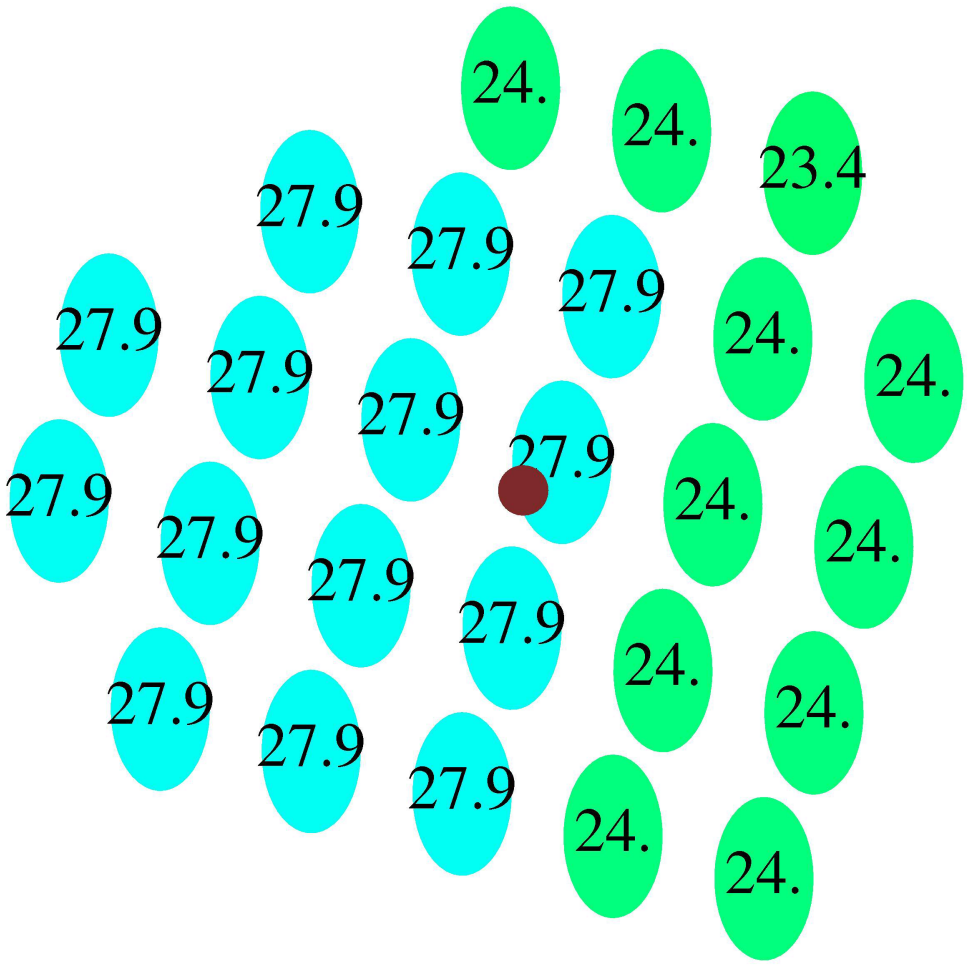
24.
24.
23.4
27.9
27.9
27.9
27.9
27.9
24.
24.
27.9
27.9
27.9
27.9
24.
24.
27.9
27.9
27.9
27.9
24.
24.
27.9
27.9
27.9
24.
24.
24.

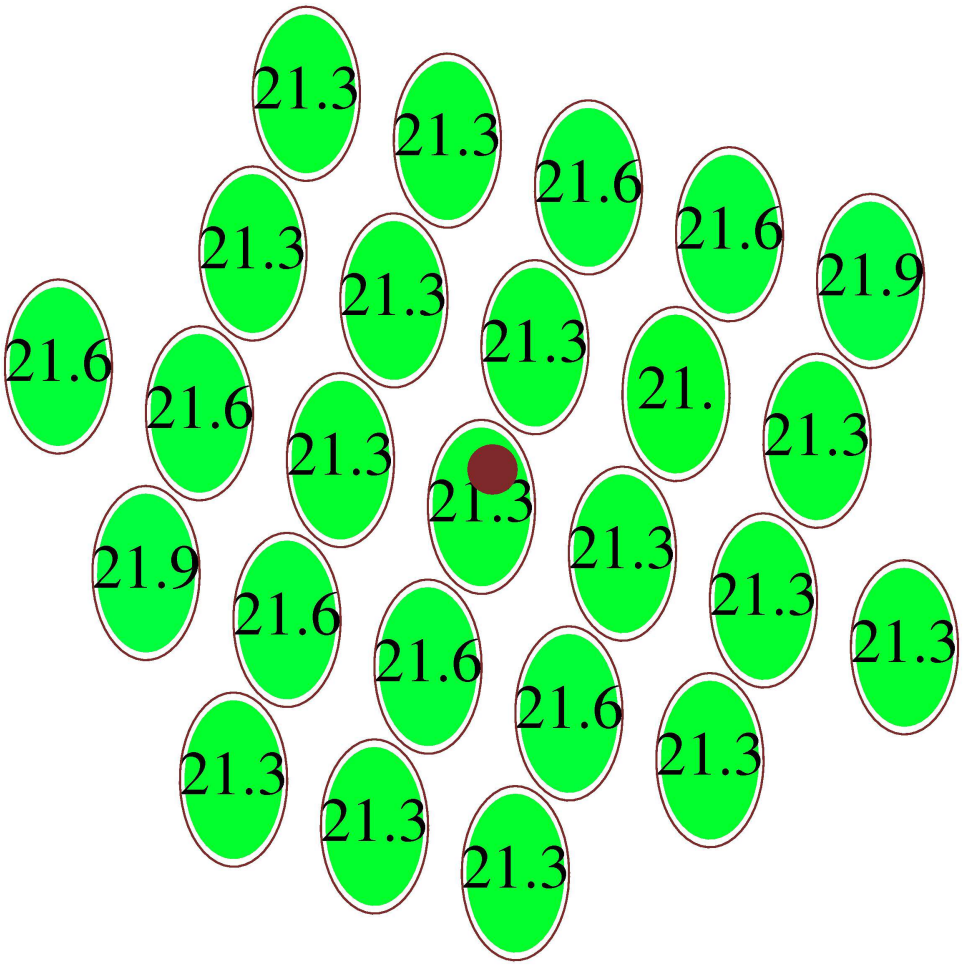
21.3
21.3
21.6
21.6
21.9
21.3
21.3
21.3
21.6
21.6
21.
21.3
21.3
21.3
21.9
21.3
21.6
21.6
21.3
21.6
21.3
21.3
21.3
21.3

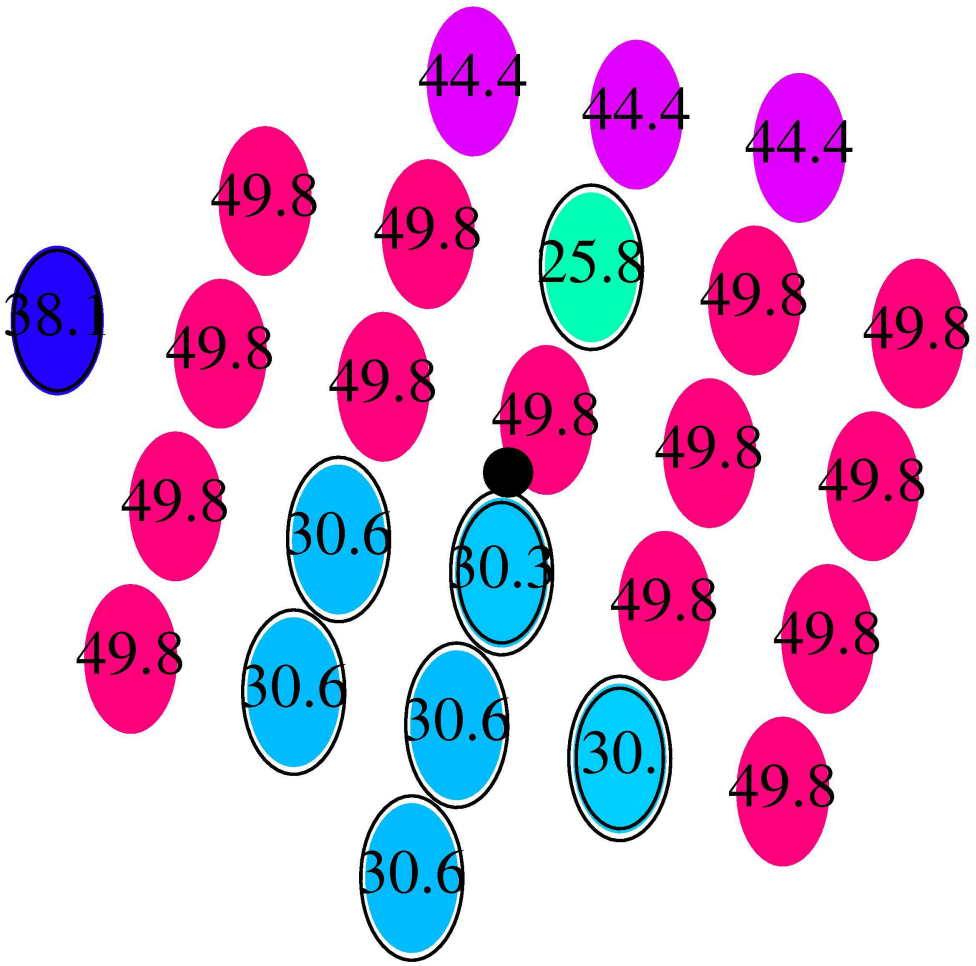
44.4
44.4
44.4
49.8
49.8
25.8
49.8
49.8
38.1
49.8
49.8
49.8
49.8
49.8
49.8
49.8
30.6
30.3
49.8
49.8
49.8
30.6
30.6
30.
49.8
30.6